

Electrically switchable non-relativistic Zeeman spin splittings in collinear antiferromagnets

Longju Yu,¹ Hong Jian Zhao,^{1,2,3,4} Laurent Bellaiche,^{5,6} and Yanming Ma^{1,3,4}

¹Key Laboratory of Material Simulation Methods and Software of Ministry of Education, College of Physics, Jilin University, Changchun 130012, China

²Key Laboratory of Physics and Technology for Advanced Batteries (Ministry of Education), College of Physics, Jilin University, Changchun 130012, China

³State Key Laboratory of High Pressure and Superhard Materials, College of Physics, Jilin University, Changchun 130012, China

⁴International Center of Future Science, Jilin University, Changchun 130012, China

⁵Smart Ferroic Materials Center, Physics Department and Institute for Nanoscience and Engineering, University of Arkansas, Fayetteville, Arkansas 72701, USA

⁶Department of Materials Science and Engineering, Tel Aviv University, Ramat Aviv, Tel Aviv 6997801, Israel

Magnetic or electrical manipulation of electronic spin is elementary for spin-based logic, computing, and memory, where the latter is a low-power manipulation scheme. Rashba-like spin splittings stemming from spin-orbit interaction (SOI) enable electric-field manipulation of spin, but the relativistic SOI causes spin relaxations and yields dissipative transport of spin-encoded information. Recent works suggest the occurrence of electric-field switchable non-relativistic Zeeman spin splittings (NRZSSs) in collinear antiferromagnets — allowing for electrical manipulation of spin in the non-relativistic regime; yet, a theory elucidating the mechanisms for these NRZSSs and guiding the materials discovery remains missing. Here, we develop such a theory by analyzing the symmetries of spin point groups. We highlight the linear magnetoelectric and bilinear piezomagnetoelectric mechanisms for NRZSSs that depend linearly on electric field and are electrically switchable. First-principles calculations further confirm that LiMnPO₄ and NaMnP showcase such NRZSSs. Our theory provides guidelines for discovering light-element collinear antiferromagnets with electrically switchable NRZSSs, which are promising for the design of high-performance spin-based devices.

Introduction — Spintronic devices (e.g., logic, computing, and memory) are built upon the manipulation of electronic spin in solids [1–5]. Such a manipulation can be achieved by magnetic field or electric field, where the latter offers fascinating low-power devices by reducing the “Joule heating” [6–8]. In principle, electric-field manipulation of spin is enabled by electrically switchable spin splittings [9, 10]. Because of the relativistic spin-orbit interaction (SOI), dielectrics and ferroelectrics naturally host electrically switchable Rashba-like spin splittings [11–15]. As a by-product, SOI causes the so-called D’yakonov-Perel’ spin relaxation as well [16–18], which yields the spin decoherence of electrons and prevents the long-range transport of the spin-encoded information [18–21]. To suppress the D’yakonov-Perel’ spin relaxation, the proposal of electrically switchable spin splittings in the non-relativistic regime is of high necessity. Recent works suggest the possibility of achieving non-relativistic Zeeman spin splittings (NRZSSs) in collinear antiferromagnets that are switchable by an electric field [22–30]. Yet, mechanisms for such NRZSSs are elusive and selection rules for the corresponding materials discovery remain to be explored.

To address the aforementioned issues, we analyze the symmetries of spin point groups (SPGs) that are associated with collinear magnets in the non-relativistic limit. This allows us to develop a theory on electrically switchable NRZSSs in collinear antiferromagnets, and

reveal the magnetoelectric and piezomagnetoelectric mechanisms for this phenomenon. Our theory provides theoretical guidelines for screening collinear antiferromagnets with electrically switchable NRZSSs. This yields the first-principles predictions that LiMnPO₄ and NaMnP are two candidates with linear magnetoelectric NRZSSs and bilinear piezomagnetoelectric NRZSSs, respectively.

NRZSSs in collinear magnets — Without the inclusion of SOI, the electronic spin angular momentum is conserved in collinear magnets [31] and serves as a good quantum number to label the electronic eigen states therein [32–35]. In this case, each spin- and momentum-resolved eigen state is associated with an eigen energy of $\varepsilon(\mathbf{k}, s_\chi)$, where \mathbf{k} is the electronic momentum, s_χ the spin angular momentum, and χ the characteristic direction for collinear magnets (i.e., magnetic moments being along χ or $-\chi$). According to Refs. [36–39], the symmetries of non-relativistic collinear magnets can be well described by 32 ferromagnetic or ferrimagnetic SPGs and 58 antiferromagnetic SPGs. The symmetry operations in SPGs are represented by $[R_s || R_l]$, with the spin operation R_s and spatial operation R_l being separated by the “||” symbol [36, 37]. The $[R_s || R_l]$ symmetry operation links the (\mathbf{k}, s_χ) and $(R_l R_s \mathbf{k}, R_s s_\chi)$ eigen states [40], implying the $\varepsilon(\mathbf{k}, s_\chi) = \varepsilon(R_l R_s \mathbf{k}, R_s s_\chi)$ relation. At the Brillouin zone center, both $\mathbf{k} = 0$ and $R_l R_s \mathbf{k} = 0$ are valid

so that the aforementioned relation can be simplified as $\varepsilon(s_\chi) = \varepsilon(R_s s_\chi)$ by omitting \mathbf{k} .

For all the $[R_s || R_l]$ symmetry operations in ferromagnetic or ferrimagnetic SPGs, $R_s s_\chi = s_\chi$ is always true and $\varepsilon(s_\chi) = \varepsilon(-s_\chi)$ is not necessarily enforced [36, 37]. This means that non-relativistic collinear ferromagnets or ferrimagnets enable the spontaneous NRZSSs (see e.g., Refs. [33–35]). Unlike those in ferromagnetic or ferrimagnetic SPGs, the $[R_s || R_l]$ symmetry operations in an antiferromagnetic SPG can be partitioned into two subsets [34–37], namely,

$$L_+ = \{[R_s^+ || R_l^+] : R_s^+ s_\chi = s_\chi\}, \quad (1)$$

and

$$L_- = \{[R_s^- || R_l^-] : R_s^- s_\chi = -s_\chi\}. \quad (2)$$

The L_+ subset is a subgroup of the antiferromagnetic SPG, and the symmetry operations therein have no restriction on $\varepsilon(s_\chi)$. In contrast, the symmetry operations in L_- suggest the $\varepsilon(s_\chi) = \varepsilon(-s_\chi)$ degeneracy, and prevent the spontaneous NRZSSs [33–35]. On the other hand, the application of external stimuli may induce NRZSSs in non-relativistic collinear antiferromagnets. This is achieved by that such stimuli break *all* the symmetry operations in the L_- set.

Electric-field induced NRZSSs — We concentrate on the NRZSSs in nonpolar collinear antiferromagnets that are driven by external electric field. To illustrate our basic logic, we work with an antiferromagnet whose SPG is the union of L_+ and L_- sets [see Eqs. (1) and (2)]. The application of electric field E_α along α direction breaks the symmetries of the antiferromagnet (α being x , y , or z). This reduces the SPG of the antiferromagnet to the union of L_+^α and L_-^α sets, where

$$\begin{aligned} L_+^\alpha &= \{[R_s^+ || R_l^+] \in L_+ : R_l^+ E_\alpha = E_\alpha\}, \\ L_-^\alpha &= \{[R_s^- || R_l^-] \in L_- : R_l^- E_\alpha = E_\alpha\}, \end{aligned} \quad (3)$$

and the “ α ” superscript labels the symmetry reduction caused by the E_α electric field [41]. When L_-^α becomes empty, there will be no symmetry operations that enforce the $\varepsilon(s_\chi) = \varepsilon(-s_\chi)$ degeneracy — enabling the electric-field induced NRZSSs. The E_α -field-induced NRZSSs are described by the effective Hamiltonian

$$\mathcal{H} = \lambda_1 E_\alpha \sigma_\chi + \lambda_2 E_\alpha^2 \sigma_\chi + \dots, \quad (4)$$

with λ_n ($n = 1, 2, \dots$) characterizing the n _{th}-order response of the Zeeman splitting to the E_α field, and σ_χ representing the Pauli matrix along the χ direction. Eq. (4) is reminiscent of the magnetoelectric coupling, and this motivates us to name the electric-field induced NRZSSs as the magnetoelectric NRZSSs.

The L_-^α set associated with an SPG may be not empty, and a material with this SPG does not host the E_α -induced NRZSSs. In such a case, we can grow this material on an appropriate substrate so that an epitaxial $\eta_{\beta\gamma}$ strain is exerted to this material. The $\eta_{\beta\gamma}$ strain might modify the symmetry of the material, and reduce the L_- set to $L_-^{\beta\gamma} = \{[R_s^- || R_l^-] \in L_- : R_l^- \eta_{\beta\gamma} = \eta_{\beta\gamma}\}$. Applying the E_α electric field to the strained material further reduces $L_-^{\beta\gamma}$ to

$$L_-^{\beta\gamma} = \{[R_s^- || R_l^-] \in L_-^{\beta\gamma} : R_l^- E_\alpha = E_\alpha\}. \quad (5)$$

Provided that $L_-^{\alpha\beta\gamma}$ is empty but $L_-^{\beta\gamma}$ is not, the NRZSSs are created via the cooperation of E_α and $\eta_{\beta\gamma}$ [42]. Phenomenologically, such NRZSSs are described by the effective Hamiltonian

$$\mathcal{H}' = \lambda'_1 E_\alpha \eta_{\beta\gamma} \sigma_\chi + \lambda'_2 E_\alpha^2 \eta_{\beta\gamma} \sigma_\chi + \lambda'_3 E_\alpha \eta_{\beta\gamma}^2 \sigma_\chi + \dots, \quad (6)$$

with λ'_n ($n = 1, 2, \dots$) being the coupling coefficients. Eq. (6) motivates us to name this type of NRZSSs as piezomagnetolectric NRZSSs.

Linear magnetoelectric and bilinear piezomagnetolectric NRZSSs — We continue to carry out symmetry analysis and extract the SPGs that host the electric-field switchable NRZSSs, following the logics mentioned in the previous section. Our detailed analysis can be found in Sections I and II of the Supplementary Material (SM), where the SPGs hosting magnetoelectric and piezomagnetolectric NRZSSs are summarized in Tables S6 and S9 therein. As shown in Eqs. (4) and (6), the E_α -driven magnetoelectric or piezomagnetolectric NRZSSs may be rooted in $E_\alpha \sigma_\chi$, $E_\alpha \eta_{\beta\gamma} \sigma_\chi$, $E_\alpha^2 \sigma_\chi$, $E_\alpha \eta_{\beta\gamma}^2 \sigma_\chi$, or other higher-order couplings (see Tables S11 and S12 of the SM). Here, we focus on the predominant electric-field induced NRZSSs which include linear magnetoelectric NRZSSs and bilinear piezomagnetolectric NRZSSs. In Tables I and II, we collect the nonpolar collinear SPGs that enable these two types of NRZSSs.

The linear magnetoelectric NRZSSs and bilinear piezomagnetolectric NRZSSs are characterized by $\lambda_1 E_\alpha \sigma_\chi$ and $\lambda'_1 E_\alpha \eta_{\beta\gamma} \sigma_\chi$, respectively. At the Brillouin zone center, the electronic eigen energies are $\varepsilon(\pm s_\chi) = \varepsilon_0 \pm \lambda_1 E_\alpha$ or $\varepsilon(\pm s_\chi) = \varepsilon_0 \pm \lambda'_1 E_\alpha \eta_{\beta\gamma}$, with ε_0 being an energy independent of spin. When changing the electric field from E_α to $-E_\alpha$, the eigen energies become $\varepsilon(\pm s_\chi) = \varepsilon_0 \mp \lambda_1 E_\alpha$ or $\varepsilon(\pm s_\chi) = \varepsilon_0 \mp \lambda'_1 E_\alpha \eta_{\beta\gamma}$. This means that both linear magnetoelectric NRZSSs and bilinear piezomagnetolectric NRZSSs are electric-field switchable.

Materials with electric-field switchable NRZSSs — Assisted by the MAGNDATA database [43, 44], and guided by Tables I and II, we explore materials with linear magnetoelectric NRZSSs or bilinear piezomagnetolectric NRZSSs. We search for nonpolar collinear antiferromagnets composed of light elements [45], identify the

TABLE I. The nonpolar collinear SPGs that enable linear magnetoelectric NRZSSs. For an SPG associated with the $E_\alpha\sigma_\chi$ coupling, a “o” symbol is filled in the corresponding entry; Such an entry is endowed with a “-” symbol if the $E_\alpha\sigma_\chi$ coupling is not symmetrically allowed. For short, we relabel each collinear $G^{\infty m}1$ SPG as G by omitting its $^{\infty m}1$ part. As an example, the $^1m^1m^1m^{\infty m}1$ SPG (abbreviated as $^1m^1m^1m$) hosts the E_z -driven linear magnetoelectric NRZSSs via the $E_z\sigma_\chi$ coupling, but does not accommodate the E_x - or E_y -driven linear magnetoelectric NRZSSs.

SPGs	E_x	E_y	E_z	SPGs	E_x	E_y	E_z
$^1\bar{1}$	o	o	o	$^12/1m$	o	-	o
$^12/1m$	-	o	-	$^12^12^12$	-	-	o
$^12^12^12$	-	o	-	$^12^12^12$	o	-	-
$^1m^1m^1m$	o	-	-	$^1m^1m^1m$	-	o	-
$^1m^1m^1m$	-	-	o	$^1\bar{4}$	-	-	o
$^14/1m$	-	-	o	$^14^12^12$	-	-	o
$^1\bar{4}^12^1m$	-	-	o	$^14/1m^1m^1m$	-	-	o
$^1\bar{3}$	-	-	o	$^13^12$	-	-	o
$^1\bar{3}^1m$	-	-	o	$^1\bar{6}$	-	-	o
$^16/1m$	-	-	o	$^16^12^12$	-	-	o
$^1\bar{6}^1m^12$	-	-	o	$^16/1m^1m^1m$	-	-	o

SPGs for such antiferromagnets, and discover LiMnPO₄ and NaMnP as two representatives with electric-field switchable NRZSSs. The antiferromagnetic LiMnPO₄ has a Néel temperature of 34 K [46, 47] and an SPG of $^1m^1m^1m^{\infty m}1$. According to Table I, the $^1m^1m^1m^{\infty m}1$ SPG enables linear magnetoelectric NRZSSs via the $E_x\sigma_\chi$ coupling. The NaMnP material is a room-temperature antiferromagnet with a Néel temperature of 560 K [48, 49]. The SPG of NaMnP is $^14/1m^1m^1m^{\infty m}1$, and this group hosts the piezomagnetolectric NRZSSs induced by the combination of η_{xy} and E_z (see the $\eta_{xy}E_z\sigma_\chi$ coupling in Table II). To validate our analysis, we compute the band structures for LiMnPO₄ and NaMnP antiferromagnets. First of all, we neglect the SOI and carry out collinear magnetism calculations. This treats the magnetic moments of Mn in LiMnPO₄ and NaMnP as scalar quantities (see Fig. 1). On this condition, the electronic spin degree of freedom appears as unmixed spin-up $+s$ and spin-down $-s$ states, where χ in s_χ is omitted at the collinear magnetism level.

As shown in Fig. S2 of the SM, both the conduction band minimum (CBM) of LiMnPO₄ and the valence band maximum (VBM) of NaMnP locate at the Brillouin zone center. We shall focus on such two band edges in our following discussion. Under null electric field, the spin-up $\varepsilon_C(+s)$ and spin-down $\varepsilon_C(-s)$ energy levels of LiMnPO₄ are degenerate at the CBM. Applying an electric field along the x direction splits the $\varepsilon_C(+s)$

TABLE II. The nonpolar collinear SPGs that enable the bilinear piezomagnetolectric NRZSSs. The η_{xx} , η_{yy} , η_{zz} , η_{xy} , η_{yz} , and η_{zx} strains are represented by “1”, “2”, “3”, “4”, “5”, and “6” numbers, respectively. For an SPG associated with the $E_\alpha\eta_{\beta\gamma}\sigma_\chi$ coupling, the number representing the $\eta_{\beta\gamma}$ strain is filled in the corresponding entry. If an SPG enables $E_\alpha\eta_{\beta\gamma}\sigma_\chi$ and $E_\alpha\eta_{\beta'\gamma'}\sigma_\chi$ couplings, two numbers representing the $\eta_{\beta\gamma}$ and $\eta_{\beta'\gamma'}$ strains are filled in the corresponding entry, and so forth. The entry with “-” indicates that the corresponding bilinear piezomagnetolectric NRZSSs are symmetrically forbidden. In this table, we relabel each collinear $G^{\infty m}1$ SPG as G by omitting its $^{\infty m}1$ part. As an example, the $^1\bar{3}^1m^{\infty m}1$ SPG (abbreviated as $^1\bar{3}^1m$ in this table) hosts the E_x -driven bilinear piezomagnetolectric NRZSSs via $E_x\eta_{xy}\sigma_\chi$ or $E_x\eta_{zx}\sigma_\chi$ couplings, but does not accommodate the E_y - and E_z -driven bilinear piezomagnetolectric NRZSSs.

SPGs	E_x	E_y	E_z	SPGs	E_x	E_y	E_z
$^12/1m$	-	45	-	$^12/1m$	45	-	45
$^12^12^12$	6	5	-	$^12^12^12$	4	-	5
$^12^12^12$	-	4	6	$^1m^1m^1m$	-	4	6
$^1m^1m^1m$	4	-	5	$^1m^1m^1m$	6	5	-
$^1m^1m^1m$	5	6	4	$^14/1m$	56	56	-
$^14/1m$	56	56	124	$^14^12^12$	-	-	4
$^14^12^12$	6	5	12	$^14^12^12$	6	5	-
$^14^12^1m$	6	5	-	$^14^12^1m$	6	5	12
$^14/1m^1m^1m$	6	5	-	$^14/1m^1m^1m$	5	6	4
$^14/1m^1m^1m$	6	5	12	$^14/1m^1m^1m$	5	6	-
$^1\bar{3}^1m$	46	-	-	$^1\bar{3}^1m$	-	46	-
$^16/1m$	56	56	-	$^16^12^12$	4	-	-
$^16^12^12$	-	4	-	$^16^12^12$	6	5	-
$^1\bar{6}^1m^12$	5	-	-	$^1\bar{6}^1m^12$	6	-	-
$^1\bar{6}/1m^1m^1m$	6	5	-	$^1\bar{6}/1m^1m^1m$	-	4	-
$^1\bar{6}/1m^1m^1m$	4	-	-	$^1\bar{6}/1m^1m^1m$	5	6	-
$^1m^1\bar{3}$	5	6	4	$^14^13^12$	5	6	4
$^1m^1\bar{3}^1m$	5	6	4				

and $\varepsilon_C(-s)$ energy levels. To be accurate, the $\Delta_1 = \varepsilon_C(+s) - \varepsilon_C(-s)$ splittings are ∓ 23 meV for $E_x = \pm 6$ MV/cm [see Figs. 2(a) and 2(b)]. For unstrained NaMnP under null electric field, the spin-up $\varepsilon_V(+s)$ and spin-down $\varepsilon_V(-s)$ energy levels at the VBM are degenerated as well. In the presence of epitaxial strain $\eta_{xy} = 4\%$, the $\Delta_2 = \varepsilon_V(+s) - \varepsilon_V(-s)$ splittings of ± 26 meV can be created by applying E_z of ± 6 MV/cm. Figure 3 shows the Δ_1 splittings in LiMnPO₄ as a function of E_x and the Δ_2 splittings in NaMnP as a function of E_z ($\eta_{xy} = 4\%$). This confirms that both the magnetoelectric NRZSSs in LiMnPO₄ (CBM) and piezomagnetolectric NRZSSs (VBM) in NaMnP depend linearly on the corresponding electric fields, and are electrically switchable.

To complete this section, we check the relativistic

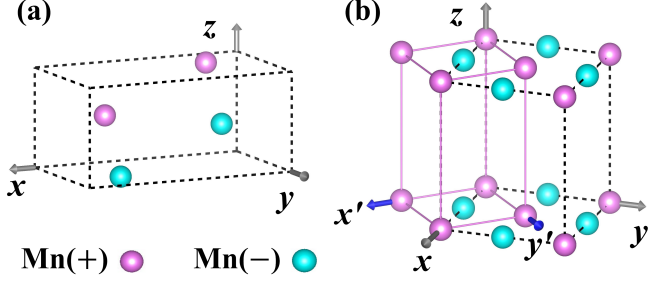


FIG. 1. Collinear magnetic structures for (a) LiMnPO₄ and (b) NaMnP antiferromagnets, where only the Mn sublattices are displayed. The cyan and pink spheres denote Mn ions with magnetic moments along $+\chi$ and $-\chi$ directions, respectively. In panels (a) and (b), the boxes enclosed by the black dashed lines represent the cells of LiMnPO₄ and NaMnP employed in our simulations. The primitive cell of NaMnP is sketched by the box with pink solid lines in panel (b).

effect on the electric-field induced Zeeman-type spin splittings in LiMnPO₄ and NaMnP. We calculate the band structures for LiMnPO₄ and NaMnP at noncollinear magnetism level (with SOI). This treats the magnetic moments of Mn as vectors along $\pm\chi$ directions ($\chi = \mathbf{x}, \mathbf{y}, \mathbf{z}$). Because of the SOI, the spin-up and spin-down eigen states are not well defined in LiMnPO₄ and NaMnP. Instead, the electronic spin degree of freedom is characterized by the spin angular momentum vector, whose predominant component is along $+\chi$ or $-\chi$ direction. In this case, we may use $\Delta'_1 = \varepsilon_C(+s_\chi) - \varepsilon_C(-s_\chi)$ and $\Delta'_2 = \varepsilon_V(+s_\chi) - \varepsilon_V(-s_\chi)$ to describe the Zeeman-type spin splittings associated with the CBM of LiMnPO₄ and the VBM of NaMnP, respectively (see the previous paragraph for the definitions of Δ_1 and Δ_2). In Fig. S3 of the SM, we show the band structures with Zeeman-type spin splittings for LiMnPO₄ and NaMnP, calculated at the relativistic level. Basically, the inclusion of relativistic corrections does not affect the magnitude of the Zeeman-type spin splittings in LiMnPO₄ and NaMnP.

Summary and outlook — By analyzing the symmetries of spin point groups, we develop a theory that describes the NRZSSs in collinear antiferromagnets driven by electric field. In particular, we identify the linear magnetoelectric and bilinear piezomagnetolectric mechanisms, both of which are associated with NRZSSs depending linearly on the applied electric field. The reversal of electric field flips the electronic spin states, yielding the electric-field switchable NRZSSs. Our central results are summarized in Tables I and II, and this guides the first-principles predictions of linear magnetoelectric NRZSSs in LiMnPO₄ and bilinear piezomagnetolectric NRZSSs in NaMnP.

Our theory provides guidelines for the discovery of light-element collinear antiferromagnets with linear mag-

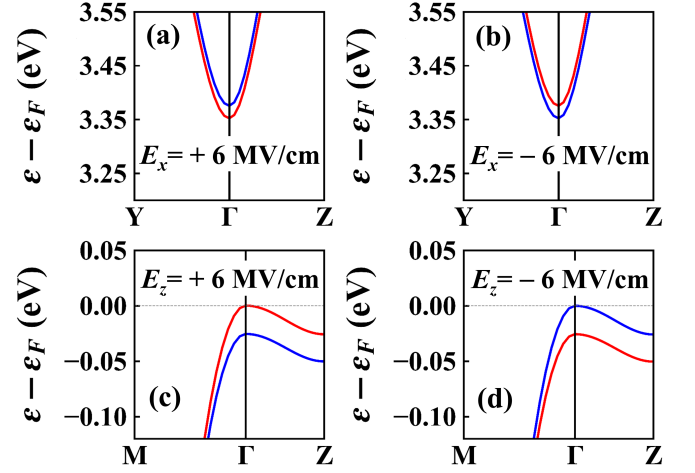


FIG. 2. The electric-field switchable NRZSSs in LiMnPO₄ and NaMnP. Panels (a) and (b) are magnetoelectric NRZSSs in LiMnPO₄ driven by E_x , while panels (c) and (d) are piezomagnetoelectric NRZSSs in NaMnP driven by E_z combined with $\eta_{xy} = 4\%$. The red (blue) solid lines correspond to the spin-up (spin-down) states, and ε_F denotes the fermi level.

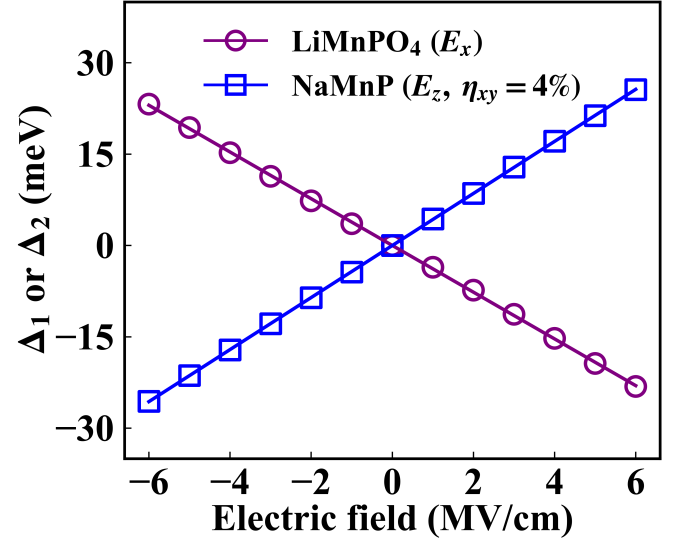


FIG. 3. The linear magnetoelectric Δ_1 splittings in LiMnPO₄ and bilinear piezomagnetoelectric Δ_2 splittings in NaMnP. Purple circles show Δ_1 in LiMnPO₄ as a function of E_x ; Blue squares show Δ_2 in NaMnP as a function of E_z (under a fixed strain of $\eta_{xy} = 4\%$). Purple and blue lines display the corresponding linear regression results.

netoelectric or bilinear piezomagnetolectric NRZSSs. The NRZSSs therein resemble Zeeman spin splittings in conventional ferromagnets or ferrimagnets, but are more attractive due to the merits of antiferromagnets (e.g., ultralow stray field and fast spin dynamics [1, 2]). Moreover, light-element materials exhibit weak SOIs that result in suppressed spin relaxations and enhanced spin life times, and the electrically switchable NRZSSs

enable the manipulation of spin in an energy-efficient electrical manner. These features highlight the potential of such light-element collinear antiferromagnets in designing high-performance spin-based information devices.

Acknowledgements — The authors acknowledge the support from the National Natural Science Foundation of China (Grants No. 12274174, No. 52288102, No. 52090024, and No. 12034009). L.B. thanks the Vannevar Bush Faculty Fellowship (VBFF) grant No. N00014-20-1-2834 from the Department of Defense and award No. DMR-1906383 from the National Science Foundation AMASE-i Program (MonArk NSF Quantum Foundry). L.Y. thanks the support from high-performance computing center of Jilin University. H.J.Z. acknowledges the support from “Xiaomi YoungScholar” Project.

-
- [1] V. Baltz, A. Manchon, M. Tsoi, T. Moriyama, T. Ono, and Y. Tserkovnyak, *Rev. Mod. Phys.* **90**, 015005 (2018).
- [2] B. H. Rimmler, B. Pal, and S. S. Parkin, *Nat. Rev. Mater.* **10**, 109 (2024).
- [3] J. Han, R. Cheng, L. Liu, H. Ohno, and S. Fukami, *Nat. Mater.* **22**, 684 (2023).
- [4] Q. L. He, T. L. Hughes, N. P. Armitage, Y. Tokura, and K. L. Wang, *Nat. Mater.* **21**, 15 (2022).
- [5] X. Lin, W. Yang, K. L. Wang, and W. Zhao, *Nat. Electron.* **2**, 274 (2019).
- [6] H. Yan, Z. Feng, P. Qin, X. Zhou, H. Guo, X. Wang, H. Chen, X. Zhang, H. Wu, C. Jiang, and Z. Liu, *Adv. Mater.* **32**, 1905603 (2020).
- [7] A. Fert, R. Ramesh, V. Garcia, F. Casanova, and M. Bibes, *Rev. Mod. Phys.* **96**, 015005 (2024).
- [8] A. Manchon, H. C. Koo, J. Nitta, S. M. Frolov, and R. A. Duine, *Nat. Mater.* **14**, 871 (2015).
- [9] L. Tao and E. Y. Tsymbal, *J. Phys. D appl. Phys.* **54**, 113001 (2021).
- [10] S. Picozzi, *Frontiers in Physics* **2**, 10 (2014).
- [11] L. L. Tao, M. Dou, X. Wang, and E. Y. Tsymbal, *Phys. Rev. Lett.* **134**, 076801 (2025).
- [12] J. Varignon, J. Santamaria, and M. Bibes, *Phys. Rev. Lett.* **122**, 116401 (2019).
- [13] P. Noël, F. Trier, L. M. Vicente Arche, J. Bréhin, D. C. Vaz, V. Garcia, S. Fusil, A. Barthélémy, L. Vila, M. Bibes, and J.-P. Attané, *Nature* **580**, 483 (2020).
- [14] F. Sheng, C. Hua, M. Cheng, J. Hu, X. Sun, Q. Tao, H. Lu, Y. Lu, M. Zhong, K. Watanabe, T. Taniguchi, Q. Xia, Z.-A. Xu, and Y. Zheng, *Nature* **593**, 56 (2021).
- [15] G. Bihlmayer, P. Noël, D. V. Vyalikh, E. V. Chulkov, and A. Manchon, *Nat. Rev. Phys.* **4**, 642 (2022).
- [16] M. I. D’yakonov and V. I. Perel’, *Sov. Phys., Solid State* **13**, 3023 (1972).
- [17] A. Manchon, J. Železný, I. M. Miron, T. Jungwirth, J. Sinova, A. Thiaville, K. Garello, and P. Gambardella, *Rev. Mod. Phys.* **91**, 035004 (2019).
- [18] M. Wu, J. Jiang, and M. Weng, *Phys. Rep.* **493**, 61 (2010).
- [19] S. Maekawa, S. O. Valenzuela, and E. Saitoh, *Spin current* (Oxford University Press, 2017).
- [20] T. Schäpers, *Semiconductor spintronics* (Walter de Gruyter GmbH & Co KG, 2021).
- [21] R. González-Hernández, L. Šmejkal, K. Vyborný, Y. Yahagi, J. Sinova, T. Jungwirth, and J. Železný, *Phys. Rev. Lett.* **126**, 127701 (2021).
- [22] S.-J. Gong, C. Gong, Y.-Y. Sun, W.-Y. Tong, C.-G. Duan, J.-H. Chu, and X. Zhang, *Proc. Natl. Acad. Sci.* **115**, 8511 (2018).
- [23] H. J. Zhao, X. Liu, Y. Wang, Y. Yang, L. Bellaiche, and Y. Ma, *Phys. Rev. Lett.* **129**, 187602 (2022).
- [24] R.-W. Zhang, C. Cui, R. Li, J. Duan, L. Li, Z.-M. Yu, and Y. Yao, *Phys. Rev. Lett.* **133**, 056401 (2024).
- [25] Y. Liu, S.-D. Guo, Y. Li, and C.-C. Liu, arXiv preprint arXiv:2502.15308 (2025).
- [26] S. Sheoran and S. Bhattacharya, *Phys. Rev. Mater.* **8**, L051401 (2024).
- [27] L. L. Tao, Q. Zhang, H. Li, H. J. Zhao, X. Wang, B. Song, E. Y. Tsymbal, and L. Bellaiche, *Phys. Rev. Lett.* **133**, 096803 (2024).
- [28] S. Sheoran and S. Bhattacharya, *Phys. Rev. B* **109**, L020404 (2024).
- [29] L.-D. Yuan, X. Zhang, C. M. Acosta, and A. Zunger, *Nat. Commun.* **14**, 5301 (2023).
- [30] Y. Chen, M. U. Farooq, and L. Huang, *Phys. Rev. B* **111**, 054418 (2025).
- [31] To design spin-based devices, spin conservation is a desired feature [19]. While spin conservation is a merit of non-relativistic collinear magnets, the occurrence of spin conservation is not guaranteed in non-relativistic noncollinear magnets (see e.g., Refs. [32–34]). The non-relativistic noncollinear magnets are thus not of interest to us.
- [32] L. Šmejkal, A. H. MacDonald, J. Sinova, S. Nakatsuji, and T. Jungwirth, *Nat. Rev. Mater.* **7**, 482 (2022).
- [33] L.-D. Yuan, Z. Wang, J.-W. Luo, and A. Zunger, *Phys. Rev. Mater.* **5**, 014409 (2021).
- [34] L. Šmejkal, J. Sinova, and T. Jungwirth, *Phys. Rev. X* **12**, 031042 (2022).
- [35] L. Šmejkal, J. Sinova, and T. Jungwirth, *Phys. Rev. X* **12**, 040501 (2022).
- [36] P. Liu, J. Li, J. Han, X. Wan, and Q. Liu, *Phys. Rev. X* **12**, 021016 (2022).
- [37] X. Chen, J. Ren, Y. Zhu, Y. Yu, A. Zhang, P. Liu, J. Li, Y. Liu, C. Li, and Q. Liu, *Phys. Rev. X* **14**, 031038 (2024).
- [38] D. B. Litvin and W. Opechowski, *Physica* **76**, 538 (1974).
- [39] D. B. Litvin, *Acta Crystallogr. Sect. A: Found. Crystallogr.* **33**, 279 (1977).
- [40] The spin operation can be written as $R_s = U_s$ or $R_s = U_s T$, with U_s and T being spin proper rotation and time reversal operation, respectively. According to Refs. [36, 37], $U_s \mathbf{k} = \mathbf{k}$ and $U_s T \mathbf{k} = -\mathbf{k}$.
- [41] When E_α is not compatible with the spatial R_l operation (i.e., $R_l E_\alpha \neq E_\alpha$), the application of E_α break the $[R_s || R_l]$ symmetry operation.
- [42] When $L_-^{\beta\gamma}$ is empty, the NRZSSs can be driven by the $\eta_{\beta\gamma}$ strain solely, without involving the E_α electric field.
- [43] S. V. Gallego, J. M. Perez-Mato, L. Elcoro, E. S. Tasci, R. M. Hanson, K. Momma, M. I. Aroyo, and G. Madariaga, *J. Appl. Crystallogr.* **49**, 1750 (2016).
- [44] S. V. Gallego, J. M. Perez-Mato, L. Elcoro, E. S. Tasci,

- R. M. Hanson, M. I. Aroyo, and G. Madariaga, *J. Appl. Crystallogr.* **49**, 1941 (2016).
- [45] The strength of SOI basically depends on the atomic mass. Materials composed of heavy elements (e.g., Bi, Sb, and Pt) likely showcase sizable SOI [50–52].
- [46] S. Gnewuch and E. E. Rodriguez, *Inorg. Chem.* **59**, 5883 (2020).
- [47] R. Toft-Petersen, N. H. Andersen, H. Li, J. Li, W. Tian, S. L. Bud'ko, T. B. S. Jensen, C. Niedermayer, M. Laver, O. Zaharko, J. W. Lynn, and D. Vaknin, *Phys. Rev. B* **85**, 224415 (2012).
- [48] W. Bronger, *Pure Appl. Chem.* **57**, 1363 (1985).
- [49] W. Bronger, P. Müller, R. Höppner, and H.-U. Schuster, *Z. Anorg. Allg. Chem.* **539**, 175 (1986).
- [50] H. Zhang, C.-X. Liu, X.-L. Qi, X. Dai, Z. Fang, and S.-C. Zhang, *Nat. Phys.* **5**, 438 (2009).
- [51] J. Li, Q. Yao, L. Wu, Z. Hu, B. Gao, X. Wan, and Q. Liu, *Nat. Commun.* **13**, 919 (2022).
- [52] L. Liu, T. Moriyama, D. Ralph, and R. Buhrman, *Phys. Rev. Lett.* **106**, 036601 (2011).